

#### **PAPER**

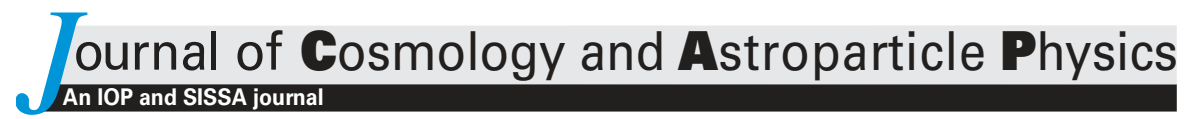
## Quasi-normal modes of loop quantum black holes formed from gravitational collapse

To cite this article: Chao Zhang and Anzhong Wang JCAP10(2024)070

View the article online for updates and enhancements.

## You may also like

- Noncommutative scalar quasinormal modes of the Reissner–Nordström black hole
- Marija Dimitrijevi iri, Nikola Konjik and Andjelo Samsarov
- Polarization-engineered AlGaN last quantum barrier for efficient deepultraviolet light-emitting diodes
   Zhongling Liu, Huabin Yu, Zhongjie Ren et al.
- Improved external quantum efficiency of deep UV LEDs with an ultra-thin AlGaN last quantum barrier by controlling the desorption-kinetics process Xiujian Sun, Jianxun Liu, Yingnan Huang et al.



RECEIVED: August 15, 2024 Accepted: September 30, 2024 Published: October 22, 2024

# Quasi-normal modes of loop quantum black holes formed from gravitational collapse

Chao Zhang  $\bigcirc a,b$  and Anzhong Wang  $\bigcirc c,*$ 

<sup>a</sup>Basic Research Center for Energy Interdisciplinary, College of Science, China University of Petroleum-Beijing, Beijing 102249, China

<sup>b</sup>Beijing Key Laboratory of Optical Detection Technology for Oil and Gas, China University of Petroleum-Beijing, Beijing 102249, China

<sup>c</sup>GCAP-CASPER, Physics Department, Baylor University, Waco, TX 76798-7316, U.S.A.

E-mail: phyzc@cup.edu.cn, anzhong\_wang@baylor.edu

ABSTRACT: In this paper, we study the quasi-normal modes (QNMs) of a scalar field in the background of a large class of quantum black holes that can be formed from gravitational collapse of a dust fluid in the framework of effective loop quantum gravity. The loop quantum black holes (LQBHs) are characterized by three free parameters, one of which is the mass parameter, while the other two are purely due to quantum geometric effects. Among these two quantum parameters, one is completely fixed by black hole thermodynamics and its effects are negligible for macroscopic black holes, while the second parameter is completely free (in principle). In the studies of the QNMs of such LQBHs, we pay particular attention to the difference of the QNMs between LQBHs and classical ones, so that they can be observed for the current and forthcoming gravitational wave observations, whereby place the LQBH theory directly under the test of observations.

Keywords: Gravitational waves in GR and beyond: theory , modified gravity, quantum black holes

ARXIV EPRINT: 2407.19654

<sup>\*</sup>Corresponding author.

$\mathbf{C}$	ontents				
1	Introduction	1			
2	LQBH background and scalar perturbation	3			
	2.1 Loop Quantum black holes formed from gravitational collapse	3			
	2.2 Perturbations of a scalar field	5			
3	Quasi-normal modes of LQBHs	7			
4 Conclusions					

#### 1 Introduction

Black holes (BHs) are one of the most mysterious phenomena in the universe. The existence of BHs provides us a perfect way to test gravitational effects under extremely strong gravitational fields, such as the formation of gigantic jets and disruption of neighboring stars. On the other hand, from the theoretical point of view, BHs are also excellent labs to test theories of gravity that are different from general relativity (GR) (see, e.g., [1–8]). It is true that BHs were initially only discovered as mathematical solutions of GR [9]. Nonetheless, observations have already confirmed their existence, including those from gravitational wave (GW) observations [10], which marks the beginning of a new era — the GW astronomy.

Following the first observation of GW, more than 90 GW events, which are all from coalescences of compact bodies, black holes and/or neutron stars, have been identified by the LIGO/Virgo/KAGRA (LVK) scientific collaborations [12–14, 16]. In the future, more advanced ground- and space-based GW detectors will be constructed [17, 18], such as Cosmic Explorer [19], Einstein Telescope [20], LISA [21], TianQin [22, 23], Taiji [24], and DECIGO [25]. These detectors will enable us to probe signals with a much wider frequency band and long distances. This has triggered the interest in the observation of quasi-normal mode (QNM) of black holes [26, 27], extreme mass ratio inspirals (EMRIs) [28, 29], the effect of dark matter on GWs [30, 31], to name only a few of them.

GWs emitted during the ringdown stage of a coalescence, where a massive black hole is just formed, can be considered as the linear combination of the QNMs of the just formed BH, and are in general studied with the perturbation theory [38–44]. QNMs of such perturbations, including scalar, vector (electromagnetic), and tensor (gravitational), have been extensively studied in GR as well as in various modified theories of gravity. From the theoretical point of view, QNMs are eigenmodes of dissipative systems and usually contain two parts, the real part and the imaginary part. Its real part gives the frequency of vibration while its

<sup>&</sup>lt;sup>1</sup>The BH just formed from the merge stage of two compact objects is highly nonlinear, and the linear perturbation theory cannot be applied to the initial stage of such just formed BH. Thus, how to connect the ringdown waveform determined by QNMs is still an open question [36, 37]. In this paper, we shall not consider such a matching, and simply consider only the times during which the GWs can be well expressed as linear combinations of QNMs.

imaginary part provides the damping time. The information contained in QNMs provide the keys in revealing whether BHs are ubiquitous in our universe, and more important whether GR is the correct theory to describe gravity even in the strong field regime. As a matter of fact, according to the no-hair theorem of GR, BHs are described uniquely by only three parameters, mass, charge and angular momentum. Thus, in GR QNMs are functions of only these three parameters. Hence, observing such modes can directly test such relations. For more details, we refer readers to [26, 27, 45, 46].

On the other hand, from the observational point of view, the sensitivities of the current detectors limit the detection of QNMs mainly to the dominant modes, and it is still an ongoing debate on whether other modes can be observed by LIGO, Virgo and KAGRA [47–54]. However, with the technological advances, it is strongly believed that the upcoming third-generation detectors, either the ground-based or the space-based ones, will be able to detect various sub-leading modes, see for example, [55] and references therein.

In this paper, we shall focus on the QNMs of a large class of quantum BHs in the context of effective loop quantum gravity (LQG) [56, 57]. It should be noted that QNMs of loop quantum black holes (LQBHs)<sup>2</sup> have been already studied extensively [29, 66–78]. However, in most of these models, the observational effects are negligible for macroscopic BHs. The LQBHs to be studied in this paper are distinguishable from the previous ones in the senses: (a) They can be directly formed from the gravitational collapse of a spherically symmetric dust cloud; and (b) the solutions usually contain three free parameters, one is the mass of the BH, and the other two characterize the quantum geometric effects. Among the two quantum parameters, one is completely fixed by the black hole thermodynamics, whose observational effects are always negligible for macroscopic BHs. On the other hand, the second quantum parameter is free [57]. Our major goal here is to study its effects to QNMs, in order to obtain observational constraints on this second quantum parameter.

The rest of the paper is organized as follows: section 2 describes briefly the LQBH solutions we are going to study in this paper and the equations for a scalar field moving in such backgrounds. The latter leads to the master equation for the study of QNMs. Knowing this, in section 3 we calculate the QNMs for both the time- and frequency-domains since the former reflects a comprehensive effect of various different modes (to be introduced below), while the latter provides a more quantitative evidence for the confinement to the coupling-parameter phase space with future GW missions. Some of our concluding remarks and future outlooks are given in section 4.

Before proceeding further, we would like to note that linear perturbations of spherically symmetric LQBH spacetimes have not been worked out yet in the framework of LQG, although some important steps were already taken [79]. In particular, the QNMs of the scalar perturbations studied in this paper cannot be compared directly with the QNMs of spin-2 gravitons of black holes studied in GR, which are directly related to the gravitational waveforms emitted in the ringdown phase [26, 27, 45, 46]. So, in this paper, what we are comparing with are the QNMs of a scalar field moving in the backgrounds of LQBHs and the QNMs of the same scalar field moving in the Schwarzschild BH background of GR, as we

 $<sup>^{2}</sup>$ Loop quantum black holes have been studied extensively in the past decades or so. For details, see [58–65] and references therein.

believe that the deviations of the scalar perturbations between these two theories are of the same order as that of the deviations of the spin-2 gravitons between the two same theories.

In addition, in this paper we are adopting the unit system so that  $c = G = \hbar = 1$ , where c denotes the speed of light, G is the gravitational constant, and  $\hbar$  the Planck constant divided by  $2\pi$ . All the Greek letter in indices run from 0 to 3. The other usages of indices will be described at suitable places.

### 2 LQBH background and scalar perturbation

In this section, we shall first introduce briefly the background of a spherically symmetric loop quantum black hole formed from the gravitational collapse of a homogeneous and isotropic dust fluid in the framework of effective theory of loop quantum gravity [56, 57], and then consider the linear perturbations of a scalar field in such backgrounds [80]. In doing so, we ignore the back-reactions of the scalar field.

#### 2.1 Loop Quantum black holes formed from gravitational collapse

The LQBH solution we are studying is given by [57]

$$ds_{+}^{2} = -f(r)dt^{2} + \frac{1}{f(r)}dr^{2} + r^{2}d\Omega^{2},$$
(2.1)

where

$$f(r) = 1 - \frac{2M}{r} + \frac{\alpha}{r^2} \left(\frac{M}{r} + \frac{B}{2}\right)^2,$$
 (2.2)

and  $d\Omega^2 = d\theta^2 + \sin^2\theta d\varphi^2$ . Here B is a dimensionless coupling parameter. Considering the above solution as describing the external spacetime of a collapsing ball, while inside the ball the spacetime is described by the FLRW universe

$$ds_{-}^{2} = -dT^{2} + a^{2} \left( dR^{2} + \chi_{k}^{2}(R) d\Omega^{2} \right), \qquad (2.3)$$

it was found that the junction conditions lead to [57]

$$B = -k\chi_k^2(R_0) = \begin{cases} -\sin^2(R_0), & k = 1, \\ 0, & k = 0, \\ \sinh^2(R_0), & k = -1, \end{cases}$$
(2.4)

where  $R_0$  denotes the junction surface. The factor  $\alpha$ , which has the dimension of  $r^2$ , is given by [57, 81]

$$\alpha = 16\sqrt{3}\pi\gamma^3\ell_{\rm pl}^2,\tag{2.5}$$

where  $\ell_{\rm pl}$  denotes the Planck length, and  $\gamma$  is known as the Barbero-Immirzi parameter whose value is set to  $\gamma \approx 0.2375$  using black hole thermodynamics in LQG [82].

To calculate QNMs of the above BHs, let us first introduce the dimensionless coordinates  $\tilde{t}$  and  $\tilde{r}$ 

$$t = r_s \tilde{t}, \quad r = r_s \tilde{r}, \tag{2.6}$$

where  $r_s \equiv 2M$ . Then, in terms of  $\tilde{t}$  and  $\tilde{r}$ , the metric reduces to

$$ds_{+}^{2} = r_{s}^{2} \left( -f(\tilde{r})d\tilde{t}^{2} + \frac{d^{2}\tilde{r}}{f(\tilde{r})} + \tilde{r}^{2}d^{2}\Omega \right)$$

$$\equiv r_{s}^{2}d\tilde{s}^{2}, \tag{2.7}$$

where

$$f(\tilde{r}) = 1 - \frac{1}{\tilde{r}} + \frac{\tilde{\alpha}}{\tilde{r}^2} \left(\frac{1}{\tilde{r}} + B\right)^2,$$

$$\tilde{\alpha} \equiv \frac{\alpha}{4r_s^2} = \sqrt{3}\pi\gamma^3 \left(\frac{\ell_{\rm pl}}{M}\right)^2.$$
(2.8)

Note that for solar-mass BHs, we have  $M \simeq 10^{38} \ \ell_{\rm pl}$ , so that (the dimensionless)  $\tilde{\alpha} \simeq \mathcal{O}\left(10^{-77}\right)$ . That is, for macroscopic BHs, the quantum gravitational effects from the  $\alpha$  terms are negligible, unless the combination of  $\tilde{\alpha}B$  is large, a condition that we will assume in order to compare the resultant QNMs of LQBHs with GW observations. Considering eq. (2.4), we find that this is possible only when k=-1. As a result, the values of B to be considered will be a non-negative number.

On the other hand, since  $ds_+^2$  and  $d\tilde{s}^2$  are related conformally with a constant conformal factor [cf., (2.7)], the physics of the spacetimes of  $ds_+^2$  can be obtained directly from that of the spacetimes of  $d\tilde{s}^2$ . In particular, by following the same manner of definition, we have  $R = \tilde{R}/r_s^2$  and

$$\tilde{\omega} \equiv r_s \omega,$$
 (2.9)

where  $\omega$  and the dimensionless  $\tilde{\omega}$  are the QNMs of  $ds_+^2$  and  $d\tilde{s}^2$ , respectively, and R and  $\tilde{R}$  are their corresponding curvatures.<sup>3</sup> Therefore, in the rest of the paper we shall work with the spacetime described by  $d\tilde{s}^2$ , i.e.

$$d\tilde{s}^2 = -f(\tilde{r})d\tilde{t}^2 + \frac{d^2\tilde{r}}{f(\tilde{r})} + \tilde{r}^2 d^2\Omega, \qquad (2.10)$$

when we calculate the QNMs of the quantum BHs. Then, using eq. (2.9) we can easily read off  $\omega$  for a given BH with mass M.

Moreover, by looking at eq. (2.2), we immediately notice that a positive radius of the metric horizon  $r_{MH}$ , which is defined through  $f(r=r_{MH})=0$ , is absent at the  $M\to 0$  limit. Therefore, by requiring  $r_{MH}>0$ , we have to look at the cases where M is large enough. Keeping this in mind, in this paper we shall consider the cases of  $\lambda \equiv M/M_{\odot} \in (3,100)^4$  in this current paper, where  $M_{\odot}$  denotes the solar mass.

<sup>&</sup>lt;sup>3</sup>One should avoid confusing the curvature R in here with the R coordinate appearing in (2.3).

<sup>&</sup>lt;sup>4</sup>In order to study their observational results, in this paper we mainly consider BHs with masses in the order of the solar mass or larger. In particular, the current GW observations set the lower limit to about  $3M_{\odot}$  (See., e.g., [83]), which makes it reasonable for us to consider the range  $M/M_{\odot} \in (3, 100)$ . As will be seen later, the difference on QNMs between a LQBH and a Schwarzschild BH sensitively depends on the ratio  $M/M_{\odot}$  when that is relatively small. After it has reached to about 100 (and even before that), the difference is observationally negligible. That is why we set the upper limit to 100 in here.

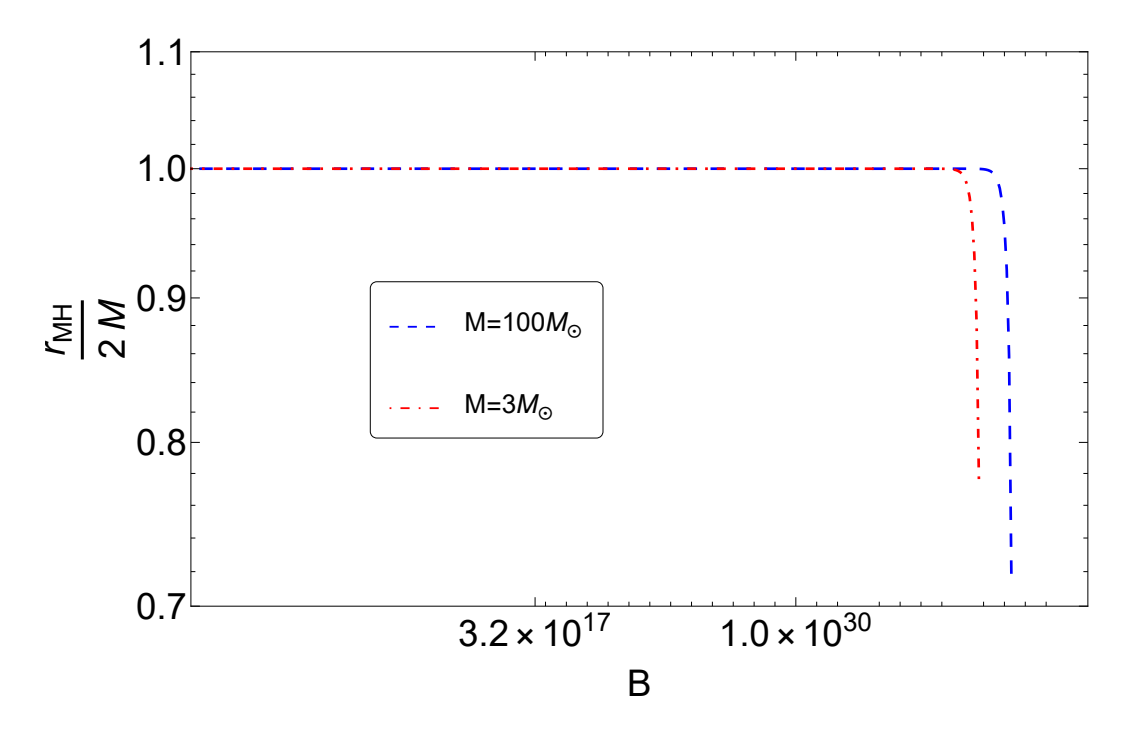


**Figure 1.** The behavior of the dimensionless quantity  $r_{MH}/(2M)$  as a function of B for different values of M.

Knowing this, we are on the position of determining an approximate upper limit for B by requiring  $r_{MH} > 0$  for  $\lambda \in (3, 100)$ . By plotting out the behavior of  $r_{MH}$  as a function of B for the range of M under consideration in figure 1, we can notice an approximate upper limit of B. A more careful study to the equation  $f(r = r_{MH}) = 0$  shows that, for a positive  $r_{MH}$  to exist for any  $\lambda \in (3, 100)$ , the upper limit of B is about  $B_{\text{max}} \approx 7.176 \times 10^{38}$ . It is worth mentioning here that, to avoid confusions arising by using different unit systems, in figure 1 we are focusing on the dimensionless quantity  $r_{MH}/(2M)$  (instead of the quantity  $r_{MH}$  itself). Therefore, the curves of figure 1 will not be changed when considering different unit systems.

In addition, by observing figure 1, we also notice that the value of  $r_{MH}/(2M)$  will soon deviate from that of GR when B reaches a critical point (For the  $M/M_{\odot}=3$  case, that critical point is located around  $B=10^{38}$ , which is very close to the upper limit of B). Before getting close to such a critical point, it is very hard to distinguish the value of  $r_{MH}/(2M)$  from its GR counterpart. This implies that one may find the observable difference between a LQBH and a Schwarzschild one only for sufficiently large B's (which should be quite close to  $B_{\text{max}}$ ). Yet, such a critical point is getting larger and larger as M increases. Therefore, given an overall  $B_{\text{max}}$  (obtained from the  $M/M_{\odot}=3$  case), we expect to barely see deviations between a LQBH and the corresponding Schwarzschild one for very large M's. We shall come back to these points later.

#### 2.2 Perturbations of a scalar field

Since in the rest of this paper we shall work only with the background described by the metric (2.10) and the dimensionless coordinates  $\tilde{t}$  as well as  $\tilde{r}$ , without causing any confusion, we shall drop the tildes from the dimensionless coordinates  $(\tilde{t}, \tilde{r})$  and the corresponding

quantities. Then, following [69] we consider the scalar perturbations that obey the Klein-Gordon equation<sup>5</sup>

$$\frac{1}{\sqrt{-g}}\partial_{\mu}\left(\sqrt{-g}g^{\mu\nu}\partial_{\nu}\Phi\right) = 0,\tag{2.11}$$

where  $\Phi = \Phi(t, r, \theta, \varphi)$  denotes the scalar field. By decomposing it through the spherical harmonics  $Y_{lm}(\theta, \varphi)$  as  $\Phi = Y_{lm}\Psi(t, r)/r$ , a master equation of  $\Psi$  is obtained as

$$\frac{\partial^2}{\partial x^2}\Psi + \left(-\frac{\partial^2}{\partial t^2} + V_{\text{eff}}(r)\right)\Psi = 0, \tag{2.12}$$

where the effective potential  $V_{\rm eff}$  is given by

$$V_{\text{eff}} \equiv f \frac{L}{r^2} + \frac{1}{2r} \frac{df^2}{dr},$$
 (2.13)

with  $L \equiv l(l+1)$ , and x the tortoise coordinate defined through

$$\frac{dr}{dx} = f(r). (2.14)$$

Notice that, since r is dimensionless, x is actually also dimensionless. Also notice that, when the background has spherical symmetry, the perturbations are independent of the choice of the angular index m [44]. Thus, without loss of the generality, we shall set m = 0. For a given function f(r) and choosing a suitable value of l, we can solve (2.12) for  $\Psi$  (which contains the information of QNMs) for a BH.

In fact, the behavior of  $V_{\rm eff}$  is directly related to the results of QNMs. Therefore, to take a glance to the influence of  $\{B,\lambda\}$  on the consequence, we first check their influence on  $V_{\rm eff}(r)$ . The behavior of  $V_{\rm eff}$  is plotted in figure 2 by setting l=2. In the upper panel we fix  $\lambda = M/M_{\odot} = 3$  and plot out different curves with a varying B factor. In contrast, in the lower panel we fix  $B = B_{\rm max} = 7.176 \times 10^{38}$  and plot out different curves with a varying  $\lambda \in (3,100)$ . Notice that, the  $V_{\rm eff}$  from GR is added to there as a comparison.

The upper panel of figure 2 implies that an observable deviation between a LQBH and a Schwarzschild one requires an extremely large B, which is consistent with what we observed from figure 1. On the other hand, as expected (again by observing figure 1), the lower panel reflects that the deviation on  $V_{\rm eff}$  from its GR counterpart will soon fade away once  $\lambda$  becomes relatively large (e.g., when it is larger than 20), even with  $B = B_{\rm max}$ . From the qualitative point of view, figure 2 provides us with a good reference on choosing the parameters from the phase space of  $\{B, \lambda\}$  when calculating for QNMs in the next section. Although we are not going to follow figure 2's choices precisely, that gives some hints to the choice of the parameters.

<sup>&</sup>lt;sup>5</sup>In this paper, we consider only the relativistic dispersion relation. In principle, higher-order corrections can be also included. But, these high-order terms are of order of  $\mathcal{O}(K^n/M_{pl}^{n-2})$  with  $n \geq 4$ , where K denotes the curvature of the macroscopic BHs, which is quite lower than the Planck scale,  $M_{pl} \gg K$  outsides of such macroscopic BHs. Therefore, for the QNMs of macroscopic BHs, these corrections are negligible. For more details, see, for example, ref. [90] and references therein.

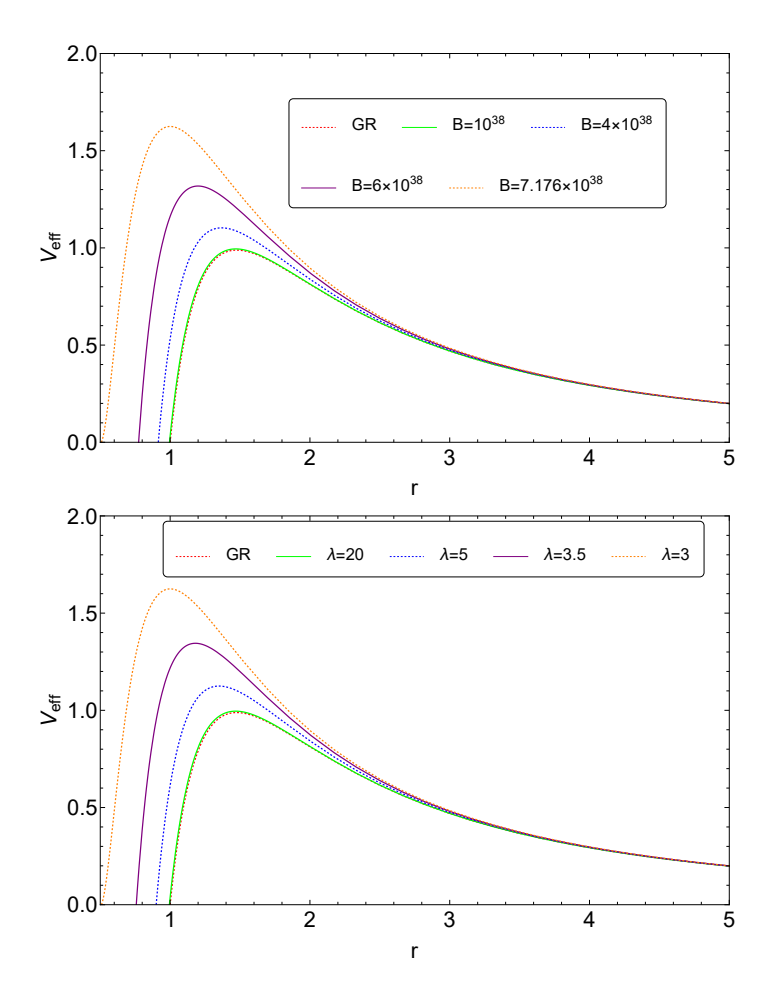


Figure 2. The behavior of  $V_{\rm eff}$  as a function of r (which is in its dimensionless form). Upper panel: for the  $\lambda = M/M_{\odot} = 3$  and l = 2 case by varying the parameter B. Lower panel: for the  $B = 7.176 \times 10^{38}$  and l = 2 case by varying the parameter  $\lambda$ . The GR case is also exhibited in here as a comparison.

## 3 Quasi-normal modes of LQBHs

First of all, we try to solve eq. (2.12) in the time-domain with the finite difference method (FDM) [7, 30, 84]. One advantage of such a method is that, for any chosen l, the final result from it can reflect comprehensively the influence of a bunch of different modes (represented by  $\{m, n\}$ , although m can be always set to zero in the spherical case without loss of the generality, as mentioned earlier. It must not be confused this m with the mass parameter M of the LQBHs.). To apply the FDM, we first introduce two new variables  $\mu \equiv t - x$  and  $\nu \equiv t + x$  [so that  $t = (\nu + \mu)/2$  and  $x = (\nu - \mu)/2$ ]. Therefore, on a  $(N + 1) \times (N + 1)$  lattice (where N is a positive integer that will be chosen properly according to our usage),

<sup>&</sup>lt;sup>6</sup>An important feature of the FDM is that in using it, we need the exact form of x(r), in addition to its derivative with respect to r. Therefore, according to the definition (2.14), we have to assign x an integral constant to absolutely fix it. In fact, such a constant could be chosen arbitrarily and it's independent of our results for calculating QNMs. Thus, we made a simple choice by letting x(r=2)=2, which is consistent with the general choice in GR (See e.g., [41]).

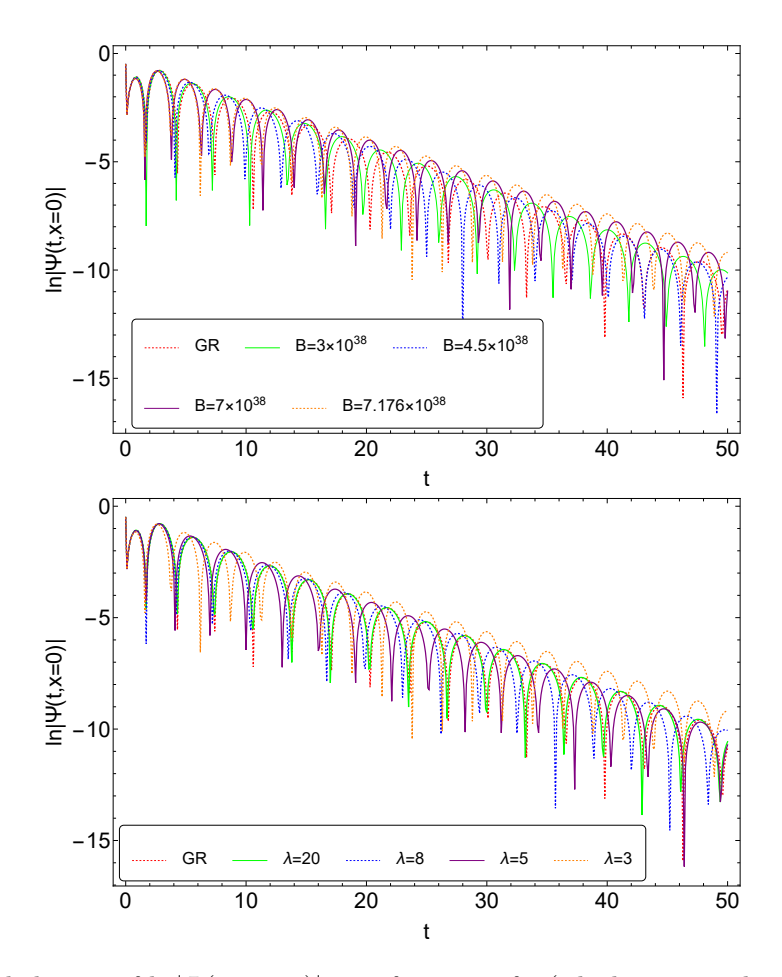


Figure 3. The behavior of  $\ln |\Psi(t, x=0)|$  as a function of t (which is in its dimensionless form). Upper panel: for the  $\lambda = M/M_{\odot} = 3$  and l=2 case with the variation of the parameter B. Lower panel: for the  $B=7.176\times 10^{38}$  and l=2 case with the variation of the parameter  $\lambda$ . The GR case is also exhibited in here as a comparison.

we perform the calculation of  $\Psi(\mu,\nu)$  by using the recursion formula

$$\Psi(\mu + \delta h, \nu + \delta h) \cong \Psi(\mu, \nu + \delta h) + \Psi(\mu + \delta h, \nu) - \Psi(\mu, \nu)$$
$$-\frac{1}{8} \delta h^2 V_{\text{eff}}(r) \left[ \Psi(\mu, \nu + \delta h) + \Psi(\mu + \delta h, \nu) \right], \tag{3.1}$$

where  $\delta h$  is the step size (which will be chosen properly in reality by measuring our tolerance of accuracy). The boundary conditions are given by  $\Psi(\mu, \nu = 0) = 0$  ( $\mu \neq 0$ ) and  $\Psi(\mu = 0, \nu) = \exp[-(\nu - 1)^2/2]$ . Thus, after  $N^2$  iterations, we find all the  $\Psi(n\delta h, n\delta h)$ 's for  $n \in [0, N] \cap \mathbb{Z}$ . From that we can calculate  $\Psi(t, x = 0)$  by using the relation  $\Psi(t, x = 0) = \Psi(\mu, \mu)$ .

Then, the results are shown in the upper panel of figure 3. For the case with  $\lambda = M/M_{\odot} = 3$  and l = 2, the behavior of  $\ln |\Psi(t, x = 0)|$  (which encodes the information of various QNM frequencies) is plotted out as a function of t for different values of B (with these values chosen by referring figure 2). It should be noted that the variable t here is dimensionless, which was previously written as  $\tilde{t} = t/r_s$ . The GR case is also added as a comparison. Just like what we have observed from figure 2, the result is not very sensitive

		GR	$\lambda = 20$			$\lambda = 10$			$\lambda = 5$		
l	n	$\omega_{GR}$	$\omega$	$\Re(\delta\omega)$	$\Im(\delta\omega)$	$\omega$	$\Re(\delta\omega)$	$\Im(\delta\omega)$	$\omega$	$\Re(\delta\omega)$	$\Im(\delta\omega)$
2	0	0.96728 - 0.19353i	0.97096 - 0.19377i	0.4%	0.1%	0.98235 - 0.19445i	1.6%	0.5%	1.03475 - 0.19666i	7.0%	1.6%
2	1	0.92769 - 0.59125i	0.93154 - 0.59191i	0.4%	0.1%	0.94349 - 0.59380i	1.7%	0.4%	0.99872 - 0.59958i	7.6%	1.4%
2	2	0.86077 - 1.01740i	0.86491 - 1.01833i	0.5%	0.1%	0.87779 - 1.02096i	2.0%	0.4%	0.93776 - 1.02794i	8.9%	1.0%
3	0	1.35073 - 0.19300i	1.35585 - 0.19324i	0.4%	0.1%	1.37173 - 0.19393i	1.6%	0.5%	1.44474 - 0.19618i	7.0%	1.6%
3	1	1.32134 - 0.58458i	1.32659 - 0.58526i	0.4%	0.1%	1.34287 - 0.58725i	1.6%	0.4%	1.41799 - 0.59356i	7.3%	1.5%
3	2	1.26718 - 0.99202i	1.27267 - 0.99308i	0.4%	0.1%	1.28971 - 0.99612i	1.8%	0.4%	1.36870 - 1.00519i	8.0%	1.3%
6	0	2.50377 - 0.19261i	2.51324 - 0.19285i	0.4%	0.1%	2.54262 - 0.19354i	1.6%	0.5%	2.67774 - 0.19582i	6.9%	1.7%
6	1	2.48750 - 0.57947i	2.49705 - 0.58018i	0.4%	0.1%	2.52665 - 0.58224i	1.6%	0.5%	2.66293 - 0.58895i	7.0%	1.6%
6	2	2.45569 - 0.97120i	2.46537 - 0.97236i	0.4%	0.1%	2.49542 - 0.97572i	1.6%	0.5%	2.63397 - 0.98646i	7.3%	1.6%

**Table 1.** Various modes of  $\omega$  (in its dimensionless form, for which we dropped the "tilde" as mentioned earlier) for LQBHs with different masses that characterized by  $\lambda$ . The GR limit of  $\omega$  for each mode is provided and the percent difference with the GR limit is shown. The factor B is fixed to be  $B = 7.176 \times 10^{38}$ .

to the value of B, especially when it is not large enough, so that the deviation between the curves of GR (represented by the red dashed line) and that of the case  $B=3\times 10^{38}$  (represented by the green solid line) is still moderate. In contrast, once B reached certain critical values, the difference becomes obvious. That is why we observe a relatively large deviation between the curves of the  $B=4.5\times 10^{38}$  case (represented by the blue dashed line) and that of the  $B=7\times 10^{38}$  case (represented by the purple solid line). On the other hand, by observing the upper panel of figure 3 we also notice that the frequency of vibration is getting bigger as the factor B increases.

Similarly, we show the corresponding results when changing  $\lambda$  in the lower panel of figure 3 (with its values chosen by referring figure 2). By setting  $B = 7.176 \times 10^{38}$  and l = 2, the behavior of  $\ln |\Psi(t, x = 0)|$  is plotted out as a function of t. We also add the GR case in order to make a comparison. As we expect from figure 1, we can barely see the deviations between the curve of a LQBH with large masses (e.g., the one represented by the green solid line) and that of GR (represented by the red dashed line), even if the parameter B is chosen to be  $B_{\text{max}}$ . In contrast, given a relatively small  $\lambda$  (e.g., the one represented by the blue dashed line), we can observe a significant deviation. On the other hand, by observing the lower panel of figure 3 we also notice that the frequency of vibrations is getting bigger with the decrease of the factor  $\lambda$ .

On the other hand, eq. (2.12) can be written in its frequency-domain as [30]

$$\frac{\partial^2}{\partial x^2}\Psi + \left(\omega^2 + V_{\text{eff}}(r)\right)\Psi = 0, \tag{3.2}$$

where  $\omega$ , representing the dimensionless quantity  $\tilde{\omega}$  introduced in eq. (2.9), is the QNM frequency to be calculated. To solve for  $\omega$  from (3.2), among various existing methods (see, e.g., [85–87]), here we introduce the WKB method [30]. The QNM frequency can be calculated up to the 6th order by using

$$\omega = \sqrt{-i \left[ \left( n + \frac{1}{2} \right) + \sum_{k=2}^{6} \Lambda_k \right] \sqrt{-2V_0''} + V_0, \tag{3.3}}$$

where

$$V_0 \equiv V_{\text{eff}}|_{r=r_{\text{max}}}, \quad V_0'' \equiv \frac{dV_{\text{eff}}}{dr^2}\Big|_{r=r_{\text{max}}},$$
 (3.4)

with  $V_{\text{eff}}(r=r_{\text{max}})$  gives the maximum of  $V_{\text{eff}}$  for  $r \in (r_{MH}/r_s, \infty)$ . The expressions of  $\Lambda_k$ 's could be found in [40, 42, 43, 88]. Note that  $n=0,1,2,\ldots$ 

For the mode  $\{l, n\}$  (recall that we have set m = 0 so that it is not mentioned), some of the results of  $\omega$  are shown in table 1. In this table we fix the factor B as  $B = 7.176 \times 10^{38}$ . In addition, the GR limit, which is denoted as  $\omega_{GR}$ , is also added as a comparison. Notice that, to compare with the results given in [69], the modes with l = 2, 6 are included in table 1. To see clearly the difference between a LQBH and a classical Schwarzschild BH with the same mass, we have introduced the percent difference defined by

$$\delta\omega \equiv \frac{\omega - \omega_{GR}}{\omega_{GR}} \times 100\%, \tag{3.5}$$

with  $\Re(\delta\omega)$  and  $\Im(\delta\omega)$  denote the real and imaginary parts of  $\delta\omega$ , respectively.

From table 1 we find that the value of  $\delta\omega$  is sensitive to the choice of  $\lambda$ . Just like what we have observed in the lower panel of figure 3, a huge  $\lambda$  often results in negligible deviations on QNMs between a LQBH and a classical Schwarzschild one. More importantly, given a sufficiently large B and a reasonable  $\lambda$ , the percent difference  $\delta\omega$  can well locate in the observational window once the LIGO-Virgo-KAGRA detector network reaches its designed sensitivity [47], whereby some constraints on these LQBHs can be found from GW observations.

In addition, it is worth mentioning here that the corresponding value of  $r_{MH}$  for each  $\omega$  appearing in table 1 effectively reflects its deviation from that of GR (as implied by figure 1). Let us take the l=2 case as an example. Setting  $\lambda=5$  leads to  $r_{MH}\approx 0.90003$  while setting  $\lambda=20$  leads to  $r_{MH}\approx 0.99434$ . Clearly, the latter is quite close to that of GR, for which we have  $r_{MH}=1$  [cf., eq. 2.8], in comparing to the former. It thus makes sense to us that the former tends to bring us an potentially observable deviation from that of GR as mentioned earlier. Actually, if we enlarge our scope, we shall find that setting  $\lambda=3$  will further putting  $r_{MH}$  into approximately 0.50800, which is obviously far away from the GR case. Although we did not show it explicitly in here, one can easily find out that the corresponding  $\omega$ 's for  $\lambda=3$  are indeed tremendously different from their counterparts of GR.

#### 4 Conclusions

In this paper we have investigated QNMs of perturbations of a scalar field on the backgrounds of a large class of LQBHs, which can be formed from gravitational collapse of realistic matter [56, 57]. These solutions are characterized by three parameters, M,  $\alpha$  and B [cf. eqs. (2.4) and (2.5), where M is the mass parameter, and  $\alpha$  and B are the two quantum parameters, characterizing the quantum geometric effects of the LQBHs. To see the effects of these two quantum parameters, it is suggestive to introduce the dimensionless coordinates  $(\tilde{t}, \tilde{r})$ , as defined by eq. (2.6), for which the spacetime can be cast in the form of eq. (2.10) with

$$f(\tilde{r}) = 1 - \frac{1}{\tilde{r}} + \frac{\tilde{\alpha}}{\tilde{r}^2} \left( \frac{1}{\tilde{r}} + B \right)^2, \tag{4.1}$$

where

$$\tilde{\alpha} \equiv \frac{\alpha}{4r_s^2} = \sqrt{3}\pi\gamma^3 \left(\frac{\ell_{\rm pl}}{M}\right)^2 \simeq \mathcal{O}\left(10^{-77}\right),\tag{4.2}$$

for a solar massive LQBH,  $M \simeq 10^{38} l_{pl}$ . Therefore, when  $B \simeq 0$ , the corresponding LQBHs have negligible effects to the observations of such BHs. From eq. (2.4) it can be seen that this is indeed the case for k = 0, +1. On the other hand, for k = -1, we have  $B = \sinh^2(R_0)$ , where  $R_0$  is the geometric radius of the collapsing dust ball. Therefore, depending on  $R_0$ , the parameter B can be arbitrarily large, so that the leading term  $\tilde{\alpha}B^2/\tilde{r}^2$  appearing in  $f(\tilde{r})$  can have observational effects for macroscopic LQBHs.

Motivated by the above considerations, we have calculated the QNMs of perturbations of a scalar field in the backgrounds of the above LQBHs. In particular, we have found that they sensitively depend on the ratio  $\lambda = M/M_{\odot}$ , when B reaches a critical value, say,  $B_c$ , which is of the order of  $B_c \simeq M_{\odot}/l_{pl} \simeq 10^{38}$ , as shown in figure 2. Therefore, with  $B \simeq B_c$  one can find significant deviations between a LQBH and a Schwarzschild one, for some values of M (or  $\lambda \equiv M/M_{\odot}$ ) as one can see from figures 1 and 2.

To be comparable with observations, in this paper we have mainly focused on the cases  $\lambda \in (3,100)$ . For such an interval of the LQBH masses, there exists an upper bound  $B_{\rm max}$  of B, only under which LQBHs exist. We have found that this maximal value is  $B_{\rm max} \approx 7.176 \times 10^{38}$ . On the other hand, we have also found that, working with the dimensionless coordinates  $(\tilde{t}, \tilde{r})$  can significantly simplify the calculations of the QNMs of the LQBHs. With this in mind, we have first studied the perturbations of the time-domain master equation (2.12). Using the FDM method [cf., (3.1)], we have solved the equation and plotted the behavior of  $|\Psi(t, x = 0)|$  as a function of  $\tilde{t}$  in figure 3 (in which simply written as t) for the dominant mode l = 2. In the upper panel of this figure, we have fixed  $\lambda = 3$ , while varying the parameter B. On the other hand, in the lower panel, we have fixed  $B = 7.176 \times 10^{38}$  but now varying  $\lambda$ . Then, we have shown that only in the neighborhood of  $(B, \lambda) \approx (B_c, 3)$  in the phase space, can the deviations of the QNMs between LQBHs and the corresponding classical BH become significant.

To find out more details, we have further calculated explicitly the values of  $\omega$  by solving the master equation in the frequency-domain [cf., (3.2)]. The corresponding results are exhibited in table 1. By examining the percent difference between the classical and LQG BHs, defined by (3.5), we have shown that the percent difference as large as 2% (or larger) can be obtained for various choices of  $\{B, \lambda\}$ . These differences could be well within the detectability of the forthcoming third-generation detectors of GWs [49, 55], whereby one can either rule out some regions of the phase space of the LQBHs or confirm them.

Finally, we note that our current work can be extended to several different directions. For instance, one may study the QNMs of other LQBHs considered in [60–62]. On the other hand, one may study the QNMs of metric perturbations of LQBHs recently developed in [79].

## Acknowledgments

We thank Profs. J. Lewandowski and P. Singh for valuable discussions on loop quantum black holes. We also thank Dr. Kai Lin for valuable discussions on the calculations of QNMs. C.Z. is supported in part by the National Natural Science Foundation of China under Grant No. 12205254, and the Science Foundation of China University of Petroleum, Beijing under Grant No. 2462024BJRC005. A.W. is partially supported by the US National Science Foundation (NSF) through the grant: PHY-2308845.

#### References

- [1] E. Berti et al., Testing general relativity with present and future astrophysical observations, Class. Quant. Grav. 32 (2015) 243001 [arXiv:1501.07274] [INSPIRE].
- [2] L. Barack et al., Black holes, gravitational waves and fundamental physics: a roadmap, Class. Quant. Grav. 36 (2019) 143001 [arXiv:1806.05195] [INSPIRE].
- [3] LIGO SCIENTIFIC et al. collaborations, Tests of general relativity with GWTC-3, arXiv:2112.06861 [INSPIRE].
- [4] X. Zhao et al., Gravitational waveforms and radiation powers of the triple system PSR J0337+1715 in modified theories of gravity, Phys. Rev. D 100 (2019) 083012 [arXiv:1903.09865] [INSPIRE].
- [5] C. Zhang et al., Gravitational waves from the quasicircular inspiral of compact binaries in Einstein-aether theory, Phys. Rev. D 101 (2020) 044002 [Erratum ibid. 104 (2021) 069905] [arXiv:1911.10278] [INSPIRE].
- [6] C. Zhang et al., Spherically symmetric static black holes in Einstein-aether theory, Phys. Rev. D 102 (2020) 064043 [arXiv:2004.06155] [INSPIRE].
- [7] C. Zhang, A. Wang and T. Zhu, Odd-parity perturbations of the wormhole-like geometries and quasi-normal modes in Einstein-aether theory, JCAP 05 (2023) 059 [arXiv:2303.08399] [INSPIRE].
- [8] Z. Carson and K. Yagi, Probing Einstein-dilaton Gauss-Bonnet gravity with the inspiral and ringdown of gravitational waves, Phys. Rev. D 101 (2020) 104030 [arXiv:2003.00286] [INSPIRE].
- K. Schwarzschild, On the gravitational field of a mass point according to Einstein's theory, Sitzungsber. Preuss. Akad. Wiss. Berlin (Math. Phys.) 1916 (1916) 189 [physics/9905030]
   [INSPIRE].
- [10] LIGO Scientific and Virgo collaborations, Observation of gravitational waves from a binary black hole merger, Phys. Rev. Lett. 116 (2016) 061102 [arXiv:1602.03837] [INSPIRE].
- [11] E. Berti et al., Spectroscopy of Kerr black holes with earth- and space-based interferometers, Phys. Rev. Lett. 117 (2016) 101102 [arXiv:1605.09286] [INSPIRE].
- [12] LIGO SCIENTIFIC and VIRGO collaborations, GWTC-1: a gravitational-wave transient catalog of compact binary mergers observed by LIGO and Virgo during the first and second observing runs, Phys. Rev. X 9 (2019) 031040 [arXiv:1811.12907] [INSPIRE].
- [13] LIGO SCIENTIFIC and VIRGO collaborations, Open data from the first and second observing runs of Advanced LIGO and Advanced Virgo, SoftwareX 13 (2021) 100658 [arXiv:1912.11716] [INSPIRE].
- [14] LIGO SCIENTIFIC and VIRGO collaborations, GW190425: observation of a compact binary coalescence with total mass  $\sim 3.4 M_{\odot}$ , Astrophys. J. Lett. 892 (2020) L3 [arXiv:2001.01761] [INSPIRE].
- [15] LIGO webpage, https://www.ligo.caltech.edu.

- [16] KAGRA et al. collaborations, GWTC-3: compact binary coalescences observed by LIGO and Virgo during the second part of the third observing run, Phys. Rev. X 13 (2023) 041039 [arXiv:2111.03606] [INSPIRE].
- [17] C.J. Moore, R.H. Cole and C.P.L. Berry, *Gravitational-wave sensitivity curves*, *Class. Quant. Grav.* **32** (2015) 015014 [arXiv:1408.0740] [INSPIRE].
- [18] Y. Gong, J. Luo and B. Wang, Concepts and status of Chinese space gravitational wave detection projects, Nature Astron. 5 (2021) 881 [arXiv:2109.07442] [INSPIRE].
- [19] Cosmic Explorer webpage, https://cosmicexplorer.org.
- [20] Einstein Telescope (ET) webpage, https://www.et-gw.eu/.
- [21] LISA the Laser Interferometer Space Antenna webpage, https://www.lisamission.org.
- [22] S. Liu, Y.-M. Hu, J.-D. Zhang and J. Mei, Science with the TianQin observatory: preliminary results on stellar-mass binary black holes, Phys. Rev. D 101 (2020) 103027 [arXiv:2004.14242] [INSPIRE].
- [23] C. Shi et al., Science with the TianQin observatory: preliminary results on testing the no-hair theorem with ringdown signals, Phys. Rev. D 100 (2019) 044036 [arXiv:1902.08922] [INSPIRE].
- [24] W.-H. Ruan, Z.-K. Guo, R.-G. Cai and Y.-Z. Zhang, Taiji program: gravitational-wave sources, Int. J. Mod. Phys. A 35 (2020) 2050075 [arXiv:1807.09495] [INSPIRE].
- [25] S. Kawamura et al., Current status of space gravitational wave antenna DECIGO and B-DECIGO, PTEP 2021 (2021) 05A105 [arXiv:2006.13545] [INSPIRE].
- [26] E. Berti, V. Cardoso and A.O. Starinets, Quasinormal modes of black holes and black branes, Class. Quant. Grav. 26 (2009) 163001 [arXiv:0905.2975] [INSPIRE].
- [27] E. Berti, K. Yagi, H. Yang and N. Yunes, Extreme gravity tests with gravitational waves from compact binary coalescences: (II) ringdown, Gen. Rel. Grav. 50 (2018) 49 [arXiv:1801.03587] [INSPIRE].
- [28] C. Zhang, Y. Gong, D. Liang and B. Wang, Gravitational waves from eccentric extreme mass-ratio inspirals as probes of scalar fields, JCAP 06 (2023) 054 [arXiv:2210.11121] [INSPIRE].
- [29] Z.-Y. Tu, T. Zhu and A. Wang, Periodic orbits and their gravitational wave radiations in a polymer black hole in loop quantum gravity, Phys. Rev. D 108 (2023) 024035 [arXiv:2304.14160] [INSPIRE].
- [30] C. Zhang, T. Zhu, X. Fang and A. Wang, Imprints of dark matter on gravitational ringing of supermassive black holes, Phys. Dark Univ. 37 (2022) 101078 [arXiv:2201.11352] [INSPIRE].
- [31] Z. Shen, A. Wang, Y. Gong and S. Yin, Analytical models of supermassive black holes in galaxies surrounded by dark matter halos, Phys. Lett. B 855 (2024) 138797 [arXiv:2311.12259] [INSPIRE].
- [32] R.A. Konoplya, How to tell the shape of a wormhole by its quasinormal modes, Phys. Lett. B 784 (2018) 43 [arXiv:1805.04718] [INSPIRE].
- [33] S.H. Völkel and K.D. Kokkotas, Wormhole potentials and throats from quasi-normal modes, Class. Quant. Grav. 35 (2018) 105018 [arXiv:1802.08525] [INSPIRE].
- [34] J.Y. Kim, C.O. Lee and M.-I. Park, Quasi-normal modes of a natural AdS wormhole in Einstein-Born-Infeld gravity, Eur. Phys. J. C 78 (2018) 990 [arXiv:1808.03748] [INSPIRE].

- [35] E. Franzin et al., Scalar perturbations around rotating regular black holes and wormholes: quasinormal modes, ergoregion instability, and superradiance, Phys. Rev. D 105 (2022) 124051 [arXiv:2201.01650] [INSPIRE].
- [36] M.H.-Y. Cheung et al., Nonlinear effects in black hole ringdown, Phys. Rev. Lett. 130 (2023) 081401 [arXiv:2208.07374] [INSPIRE].
- [37] K. Mitman et al., Nonlinearities in black hole ringdowns, Phys. Rev. Lett. 130 (2023) 081402 [arXiv:2208.07380] [INSPIRE].
- [38] T. Regge and J.A. Wheeler, Stability of a Schwarzschild singularity, Phys. Rev. 108 (1957) 1063 [INSPIRE].
- [39] S.A. Teukolsky, Perturbations of a rotating black hole. 1. Fundamental equations for gravitational electromagnetic and neutrino field perturbations, Astrophys. J. 185 (1973) 635 [INSPIRE].
- [40] B.F. Schutz and C.M. Will, Black hole normal modes: a semianalytic approach, Astrophys. J. Lett. 291 (1985) L33 [INSPIRE].
- [41] E.W. Leaver, An analytic representation for the quasi normal modes of Kerr black holes, Proc. Roy. Soc. Lond. A 402 (1985) 285 [INSPIRE].
- [42] S. Iyer and C.M. Will, Black hole normal modes: a WKB approach. 1. Foundations and application of a higher order WKB analysis of potential barrier scattering, Phys. Rev. D 35 (1987) 3621 [INSPIRE].
- [43] S. Iyer, Black hole normal modes: a WKB approach. 2. Schwarzschild black holes, Phys. Rev. D 35 (1987) 3632 [INSPIRE].
- [44] S. Chandrasekhar, *The mathematical theory of black holes*, Oxford University Press, Oxford, U.K. (1992).
- [45] I. Muller, Speeds of propagation in classical and relativistic extended thermodynamics, Living Rev. Rel. 2 (1999) 1 [INSPIRE].
- [46] R.A. Konoplya and A. Zhidenko, Quasinormal modes of black holes: from astrophysics to string theory, Rev. Mod. Phys. 83 (2011) 793 [arXiv:1102.4014] [INSPIRE].
- [47] G. Carullo et al., Empirical tests of the black hole no-hair conjecture using gravitational-wave observations, Phys. Rev. D 98 (2018) 104020 [arXiv:1805.04760] [INSPIRE].
- [48] M. Isi et al., Testing the no-hair theorem with GW150914, Phys. Rev. Lett. 123 (2019) 111102 [arXiv:1905.00869] [INSPIRE].
- [49] J. Calderón Bustillo, P.D. Lasky and E. Thrane, Black-hole spectroscopy, the no-hair theorem, and GW150914: Kerr versus Occam, Phys. Rev. D 103 (2021) 024041 [arXiv:2010.01857] [INSPIRE].
- [50] E. Finch and C.J. Moore, Searching for a ringdown overtone in GW150914, Phys. Rev. D 106 (2022) 043005 [arXiv:2205.07809] [INSPIRE].
- [51] S. Ma, L. Sun and Y. Chen, Using rational filters to uncover the first ringdown overtone in GW150914, Phys. Rev. D 107 (2023) 084010 [arXiv:2301.06639] [INSPIRE].
- [52] M. Isi and W.M. Farr, Comment on "Analysis of ringdown overtones in GW150914", Phys. Rev. Lett. 131 (2023) 169001 [arXiv:2310.13869] [INSPIRE].
- [53] G. Carullo, R. Cotesta, E. Berti and V. Cardoso, Reply to comment on "Analysis of ringdown overtones in GW150914", Phys. Rev. Lett. 131 (2023) 169002 [arXiv:2310.20625] [INSPIRE].

- [54] C.D. Capano et al., Multimode quasinormal spectrum from a perturbed black hole, Phys. Rev. Lett. 131 (2023) 221402 [arXiv:2105.05238] [INSPIRE].
- [55] C. Shi, Q. Zhang and J. Mei, On the detectability and resolvability of quasi-normal modes with space-based gravitational wave detectors, arXiv:2407.13110 [INSPIRE].
- [56] J. Lewandowski, Y. Ma, J. Yang and C. Zhang, Quantum Oppenheimer-Snyder and Swiss cheese models, Phys. Rev. Lett. 130 (2023) 101501 [arXiv:2210.02253] [INSPIRE].
- [57] L. Cafaro and J. Lewandowski, Status of Birkhoff's theorem in the polymerized semiclassical regime of loop quantum gravity, Phys. Rev. D 110 (2024) 024072 [arXiv:2403.01910] [INSPIRE].
- [58] R. Gambini, J. Olmedo and J. Pullin, Quantum geometry and black holes, in Handbook of quantum gravity, C. Bambi, L. Modesto and I. Shapiro eds., Springer, Singapore (2023) [DOI:10.1007/978-981-19-3079-9\_105-1] [arXiv:2211.05621] [INSPIRE].
- [59] A. Ashtekar, J. Olmedo and P. Singh, Regular black holes from loop quantum gravity, in Handbook of quantum gravity, C. Bambi, L. Modesto and I. Shapiro eds., Springer, Singapore (2023) [arXiv:2301.01309] [INSPIRE].
- [60] G. Ongole, P. Singh and A. Wang, Revisiting quantum black holes from effective loop quantum gravity, Phys. Rev. D 109 (2024) 026015 [arXiv:2311.10166] [INSPIRE].
- [61] W.-C. Gan et al., Understanding quantum black holes from quantum reduced loop gravity, Phys. Rev. D 106 (2022) 126013 [arXiv:2206.07127] [INSPIRE].
- [62] W.-C. Gan, N.O. Santos, F.-W. Shu and A. Wang, Properties of the spherically symmetric polymer black holes, Phys. Rev. D 102 (2020) 124030 [arXiv:2008.09664] [INSPIRE].
- [63] W.-C. Gan et al., Nonexistence of quantum black and white hole horizons in an improved dynamic approach, Sci. China Phys. Mech. Astron. 67 (2024) 280411 [arXiv:2212.14535] [INSPIRE].
- [64] H. Zhang, W.-C. Gan, Y. Gong and A. Wang, On the improved dynamics approach in loop quantum black holes, Commun. Theor. Phys. 76 (2024) 035401 [arXiv:2308.15574] [INSPIRE].
- [65] G. Ongole et al., Dirac observables in the 4-dimensional phase space of Ashtekar's variables and spherically symmetric loop quantum black holes, Universe 8 (2022) 543 [arXiv:2208.10562] [INSPIRE].
- [66] J.-M. Yan et al., Observational tests of a quantum extension of Schwarzschild spacetime in loop quantum gravity with stars in the galactic center, Phys. Rev. D 107 (2023) 084043 [arXiv:2302.10482] [INSPIRE].
- [67] J.-M. Yan et al., Constraints on self-dual black hole in loop quantum gravity with S0-2 star in the galactic center, JCAP 09 (2022) 008 [arXiv:2203.03203] [INSPIRE].
- [68] Y.-C. Liu, J.-X. Feng, F.-W. Shu and A. Wang, Extended geometry of Gambini-Olmedo-Pullin polymer black hole and its quasinormal spectrum, Phys. Rev. D 104 (2021) 106001 [arXiv:2109.02861] [INSPIRE].
- [69] R.G. Daghigh, M.D. Green and G. Kunstatter, Scalar perturbations and stability of a loop quantum corrected Kruskal black hole, Phys. Rev. D 103 (2021) 084031 [arXiv:2012.13359] [INSPIRE].
- [70] A. Arbey et al., Hawking radiation by spherically-symmetric static black holes for all spins: Teukolsky equations and potentials, Phys. Rev. D 103 (2021) 104010 [arXiv:2101.02951] [INSPIRE].

- [71] E.R. Livine, C. Montagnon, N. Oshita and H. Roussille, Scalar quasi-normal modes of a loop quantum black hole, JCAP 10 (2024) 037 [arXiv:2405.12671] [INSPIRE].
- [72] Z.-W. Xia, H. Yang and Y.-G. Miao, Scalar fields around a rotating loop quantum gravity black hole: waveform, quasi-normal modes and superradiance, Class. Quant. Grav. 41 (2024) 165010 [arXiv:2310.00253] [INSPIRE].
- [73] G. Fu et al., Peculiar properties in quasinormal spectra from loop quantum gravity effect, Phys. Rev. D 109 (2024) 026010 [arXiv:2301.08421] [INSPIRE].
- [74] C.-Y. Shao, C. Zhang, W. Zhang and C.-G. Shao, Scalar fields around a loop quantum gravity black hole in de Sitter spacetime: quasinormal modes, late-time tails and strong cosmic censorship, Phys. Rev. D 109 (2024) 064012 [arXiv:2309.04962] [INSPIRE].
- [75] J. Yang, C. Zhang and Y. Ma, Shadow and stability of quantum-corrected black holes, Eur. Phys. J. C 83 (2023) 619 [arXiv:2211.04263] [INSPIRE].
- [76] M. Okounkova et al., Numerical relativity simulation of GW150914 beyond general relativity, Phys. Rev. D 101 (2020) 104016 [arXiv:1911.02588] [INSPIRE].
- [77] C. Liu et al., Shadow and quasinormal modes of a rotating loop quantum black hole, Phys. Rev. D 101 (2020) 084001 [Erratum ibid. 103 (2021) 089902] [arXiv:2003.00477] [INSPIRE].
- [78] L.-M. Cao et al., The pseudospectrum and spectrum (in)stability of quantum corrected Schwarzschild black hole, Sci. China Phys. Mech. Astron. 67 (2024) 100412 [arXiv:2401.09907] [INSPIRE].
- [79] G.A. Mena Marugán and A. Mínguez-Sánchez, Axial perturbations in Kantowski-Sachs spacetimes and hybrid quantum cosmology, Phys. Rev. D 109 (2024) 106009 [arXiv:2402.08307] [INSPIRE].
- [80] O. Stashko, Quasinormal modes and gray-body factors of regular black holes in asymptotically safe gravity, Phys. Rev. D 110 (2024) 084016 [arXiv:2407.07892] [INSPIRE].
- [81] D.-W. Chiou, Phenomenological loop quantum geometry of the Schwarzschild black hole, Phys. Rev. D 78 (2008) 064040 [arXiv:0807.0665] [INSPIRE].
- [82] K.A. Meissner, Black hole entropy in loop quantum gravity, Class. Quant. Grav. 21 (2004) 5245 [gr-qc/0407052] [INSPIRE].
- [83] LIGO SCIENTIFIC et al. collaborations, Observation of gravitational waves from the coalescence of a 2.5-4.5 M<sub>⊙</sub>< compact object and a neutron star, Astrophys. J. Lett. 970 (2024) L34 [arXiv:2404.04248] [INSPIRE].
- [84] R. Haberman, Applied partial differential equations: with Fourier series and boundary value problems, fifth edition, Pearson Education Inc., Saddle River, NJ 07458, U.S.A. (2013).
- [85] S. Chandrasekhar and S.L. Detweiler, The quasi-normal modes of the Schwarzschild black hole, Proc. Roy. Soc. Lond. A 344 (1975) 441 [INSPIRE].
- [86] K. Lin and W.-L. Qian, A matrix method for quasinormal modes: Schwarzschild black holes in asymptotically flat and (anti-) de Sitter spacetimes, Class. Quant. Grav. 34 (2017) 095004 [arXiv:1610.08135] [INSPIRE].
- [87] R. Ghosh, N. Franchini, S.H. Völkel and E. Barausse, Quasinormal modes of nonseparable perturbation equations: the scalar non-Kerr case, Phys. Rev. D 108 (2023) 024038 [arXiv:2303.00088] [INSPIRE].
- [88] R.A. Konoplya, Quasinormal behavior of the d-dimensional Schwarzschild black hole and higher order WKB approach, Phys. Rev. D 68 (2003) 024018 [gr-qc/0303052] [INSPIRE].

- [89] V. Cardoso and J.P.S. Lemos, Scalar, electromagnetic and Weyl perturbations of BTZ black holes: quasinormal modes, Phys. Rev. D 63 (2001) 124015 [gr-qc/0101052] [INSPIRE].
- [90] A. Wang, Hořava gravity at a Lifshitz point: a progress report, Int. J. Mod. Phys. D 26 (2017) 1730014 [arXiv:1701.06087] [INSPIRE].
- [91] M. Chabab, H. El Moumni, S. Iraoui and K. Masmar, Behavior of quasinormal modes and high dimension RN-AdS black hole phase transition, Eur. Phys. J. C 76 (2016) 676 [arXiv:1606.08524] [INSPIRE].
- [92] W. Wahlang, P.A. Jeena and S. Chakrabarti, Quasinormal modes of scalar and Dirac perturbations of Bardeen de-Sitter black holes, Int. J. Mod. Phys. D 26 (2017) 1750160 [arXiv:1703.04286] [INSPIRE].
- [93] R.A. Konoplya, Z. Stuchlík and A. Zhidenko, Axisymmetric black holes allowing for separation of variables in the Klein-Gordon and Hamilton-Jacobi equations, Phys. Rev. D 97 (2018) 084044 [arXiv:1801.07195] [INSPIRE].
- [94] R.G. Daghigh, M.D. Green, J.C. Morey and G. Kunstatter, Scalar perturbations of a single-horizon regular black hole, Phys. Rev. D 102 (2020) 104040 [arXiv:2009.02367] [INSPIRE].
- [95] Z. Li, Scalar perturbation around rotating regular black hole: superradiance instability and quasinormal modes, Phys. Rev. D 107 (2023) 044013 [arXiv:2210.14062] [INSPIRE].
- [96] Y.-H. Lei, Z.-H. Yang and X.-M. Kuang, Scalar field perturbation around a rotating hairy black hole: quasinormal modes, quasibound states and superradiant instability, Eur. Phys. J. C 84 (2024) 438 [arXiv:2310.05190] [INSPIRE].
- [97] J. Barragán Amado and B. Gwak, Scalar quasi-normal modes of accelerating Kerr-Newman-AdS black holes, JHEP 02 (2024) 189 [arXiv:2309.11355] [INSPIRE].
- [98] C. Zhang, A. Wang and T. Zhu, Odd-parity perturbations of the wormhole-like geometries and quasi-normal modes in Einstein-aether theory, JCAP 05 (2023) 059 [arXiv:2303.08399] [INSPIRE].